(Preprint) AAS XX-XXX

A TIME-REGULARIZED MULTIPLE GRAVITY-ASSIST LOW-THRUST BOUNDED-IMPULSE MODEL FOR TRAJECTORY OPTIMIZATION

Donald H. Ellison *
Jacob A. Englander †
Bruce A. Conway ‡

The multiple gravity assist low-thrust (MGALT) trajectory model combines the medium-fidelity Sims-Flanagan bounded-impulse transcription with a patched-conics flyby model and is an important tool for preliminary trajectory design. While this model features fast state propagation via Kepler's equation and provides a pleasingly accurate estimation of the total mass budget for the eventual flight-suitable integrated trajectory it does suffer from one major drawback, namely its temporal spacing of the control nodes. We introduce a variant of the MGALT transcription that utilizes the generalized anomaly from the universal formulation of Kepler's equation as a decision variable in addition to the trajectory phase propagation time.This results in two improvements over the traditional model. The first is that the maneuver locations are equally spaced in generalized anomaly about the orbit rather than time. The second is that the Kepler propagator now has the generalized anomaly as its independent variable instead of time and thus becomes an iteration-free propagation method. The new algorithm is outlined, including the impact that this has on the computation of Jacobian entries for numerical optimization, and a motivating application problem is presented that illustrates the improvements that this model has over the traditional MGALT transcription.

INTRODUCTION

Bounded-impulse trajectory models are an integral part of many preliminary design methodologies. For the case of continuous-thrust trajectory design, the multiple gravity-assist low-thrust (MGALT) model has been incorporated into many tool chains such as the Evolutionary Mission Trajectory Generator (EMTG), Mission Analysis Low-Thrust Optimization (MALTO),[1] Gravity-Assist Low-thrust Local Optimization Program (GALLOP)[2] and the Parallel Global Multiobjective Optimizer (PaGMO).[3] The MGALT transcription combines the medium-fidelity Sims-Flanagan bounded-impulse model,[4] which divides a trajectory phase into N equal sized time segments with a bounded-impulse placed at the center of each segment, with a patched-conics flyby model. Its strength lies in generating accurate mass budgets for interplanetary missions. MGALT optimization runs generate medium-fidelity solutions and, therefore, are typically used as seeds for higher fidelity models such as the finite-burn low-thrust (FBLT) model[5,6] and flight-grade tools such as GMAT[7] and Mystic.[8,9]

While MGALT is capable of accurately approximating many types of interplanetary trajectories, certain classes of missions such as those requiring multiple-revolutions of the central body, with no intermediate flybys, as well as those requiring large eccentricity changes present more of a challenge to this model. The more revolutions that the spacecraft requires to complete a transfer, the more control discretization nodes are required to ensure that the bounded-impulse trajectory will be suitable as a seed to a finite-burn model. For trajectories requiring large eccentricity changes, the original Sims-Flanagan model, which evenly spaces control nodes in time, places these nodes at precisely non-optimal locations. That is, for high-eccentricity orbits, the control nodes cluster around apoapsis and are sparse at periapsis where energy changes are more efficiently achieved and therefore where higher control authority is typically desirable. The only way to mitigate this shortcoming of MGALT is to add more control points, which increases the computational complexity of the problem. For this reason, a bounded-impulse transcription that requires fewer control nodes and,

[1]Ph. D. Candidate, Department of Aerospace Engineering, 104 South Wright Street, Urbana, IL, 61801, Mail Code-236, Student Member AIAA
[2]Aerospace Engineer, Navigation and Mission Design Branch, 8800 Greenbelt Rd, Greenbelt, MD 20771, Member AIAA
[3]Professor Emeritus, Department of Aerospace Engineering, 104 South Wright Street, Urbana, IL, 61801, Mail Code-236, Associate Fellow AIAA

at a minimum, results in a geometrically even distribution of the control points around the trajectory phase would be desirable.

Redistribution of the control nodes is typically achieved using a time-regularization transformation such as a Sundman transformation. This has recently been investigated by Pellegrini et al.[10] who applied generalized Sundman transformations to the Stark and Kepler (sub-case of Stark) problems. Their Stark solution method is based on a series solution, where the length of the series determines the accuracy of the solution. The Stark model was also extended for use with a Taylor integrator similar to the work by Yam et al.[11] In this paper, we introduce an exact method for solving the time-regularized Kepler problem that does not rely on a series solution. Solving Kepler's equation typically requires iterative techniques such as Newton's method, the Laguerre-Conway method or bisection. We propose a strategy that transforms a universal Kepler propagator into an iteration-free method at the expense of the introduction of one additional decision variable per trajectory phase (to be chosen by an NLP optimizer). These new variables are the total generalized anomaly to propagate the spacecraft state by in a trajectory phase (χ_p). The addition of these decision parameters results in an execution speed increase due to the elimination of numerical iteration in the propagator, and also a more favorable distribution of control nodes for highly eccentric trajectories. In addition, it is possible to compute analytic partial derivatives of the problem constraint vector $\mathbf{c}$ with respect to the χ_p variables. The redistribution of nodes using this method is a Sundman transformation,[10,12] as such we will hereafter refer to the modified model as the multiple gravity-assist low-thrust Sundman (MGALTS) transcription.

ALGORITHM

For the case of the original MGALT model, a numerical optimizer selects the phase flight time variable (Δt_p), and a Kepler solver then determines the corresponding change in eccentric anomaly, or generalized anomaly, for a universal variable formulation. When time-regularization is applied, where control nodes are distributed in a geometrically even sense along the trajectory, the angular variable (E or χ) becomes the decision variable in lieu of the flight time. This is a non-intuitive variable for the human mission designer to select, however, as any given angular displacement can result in dramatically different flight times depending on the geometry of the orbit. Requiring a mission designer to select angular displacements instead of flight times is really not feasible. An even more difficult task for a human would be to determine, *a priori*, the temporal spacing between each control node required to achieve perfect geometrical distribution of the control nodes.

Instead of each of these undesirable jobs, in this method we remove the burden of having a mission designer select the angular displacement and shift the responsibility to the NLP solver. Then, the universal Kepler solver is used in an inverse sense to compute the time-of-flight required to satisfy an even distribution of control points, in addition to propagating the state without the need for iteration. The procedure for evaluating a trajectory phase, and for obtaining all the necessary partials to compute match point derivatives, is as follows (definitions for the symbols below are provided in the Appendix):

1. χ_p is an NLP decision variable and is equal to the total generalized anomaly required to propagate one trajectory phase. The size of a propagation segment is $\Delta\chi_k = \frac{\chi_\mathrm{p}}{N}$
2. Starting at the left boundary, propagate inwards to the phase center for $\frac{N}{2}$ segments of generalized anomaly
3. For each k^{th} propagation step in the forward half-phase:
   (a) compute α_k to determine if the current conic orbit is elliptic, hyperbolic or parabolic (this affects the computation of the universal variables U_{n_k} and their derivatives)
   (b) compute the universal functions $U_{n_k} \;\; n = 0, 1, 2, 3$
   (c) compute $\frac{\partial U_{n_k}}{\partial \alpha_k}$ and $\frac{\partial U_{n_k}}{\partial \chi_k} \;\; n = 0, 1, 2, 3$ (for use in computing step g).
   (d) compute the segment propagation time Δt_k resulting from a propagation through $\Delta\chi_k$ of generalized anomaly as well as $\frac{\partial \Delta t_k}{\partial \chi_k}$
   (e) compute the Lagrange coefficients and their derivatives F_k, $\frac{\partial F_k}{\partial \chi_k}$, $\dot{F}_k$, $\frac{\partial \dot{F}_k}{\partial \chi_k}$, G_k, $\frac{\partial G_k}{\partial \chi_k}$, $\dot{G}_k$ and $\frac{\partial \dot{G}_k}{\partial \chi_k}$
   (f) compute the propagated state $\mathbf{X}_k^- = \begin{bmatrix}\mathbf{r}_k^- & \mathbf{v}_k^-\end{bmatrix}^T$
   (g) compute $\frac{\partial \mathbf{X}_k^-}{\partial \mathbf{X}_{k-1}^+}$ and $\frac{\partial \Delta t_k}{\partial \mathbf{X}_{k-1}^+}$, which form the basis for computing match-point derivatives
   (h) compute the maximum available thrust $T_{\max_k}$
   (i) compute $\Delta v_{\max_k}$

(j) compute throttle magnitude constraint $\|\mathbf{u}_k\| < 1$

(k) apply the impulsive maneuver $\mathbf{v}_k^+ = \mathbf{v}_k^- \pm \mathbf{u}_k \Delta v_{\max_k}$

(l) compute the spacecraft's mass after the applied impulse m_k^+

4. Locate the right hand phase boundary using the phase flight time NLP decision variable Δt_p

5. Repeat step 3 for the backwards half-phase

6. compute the match point constraint $\mathbf{c}^\dagger$ and its partials $\frac{\partial \mathbf{c}^\dagger}{\partial \mathbf{p}}$ (here we denote the phase match point with the dagger symbol †)

In the procedure above, the - and + superscripts indicate a quantity immediately prior to and after an applied impulse respectively. The 3x1 vector $\mathbf{u}_k$ contains the control parameters of the k^{th} segment. The scalar quantity $\Delta v_{\max_k}$ represents the maximum Δv achievable by the spacecraft over the course of the k^{th} segment:

$$\Delta v_{\max_k} = \frac{N_\mathrm{active} D \, T_{\max_k} \Delta t_k}{m_k} \tag{1}$$

In Equation (1), N_active is the number of active thrusters, D is the thruster duty cycle, $T_{\max_k}$ is the maximum available thrust for the current segment computed using the propulsion system power model[5] and m_k is the mass of the spacecraft at the left-hand side of the segment. The spacecraft's mass across the k^{th} bounded impulse is computed using the following equation:

$$m_k = \begin{cases} m_{k-1} - \|\mathbf{u}_{k-1}\| \, \Delta m_{\max_{k-1}} & \text{forward propagation} \\ m_{k+1} + \|\mathbf{u}_k\| \, \Delta m_{\max_k} & \text{backward propagation} \end{cases} \tag{2}$$

where $m_{\max_k} = D \, \Delta t \, \dot{m}_{\max_k}$ and Δt_k given by Eq. (11) in the Appendix . Note that the impulsive thrust approximation implies $m_{k-1}^+ = m_k^-$ and for notational convenience, we set $m_k^- = m_k$.

One peculiarity of this method is that the maximum size of a maneuver $\Delta v_{\max_k}$ can only be determined after the propagation time Δt_k has been computed. This is in contrast to using an equivalent time spacing of the nodes (MGALT) where segment propagation time is known prior to propagation and hence the trajectory may be computed in half-segments. For this reason, maneuvers must occur at the the right-hand boundary of a segment instead of in the middle as they would for the original MGALT transcription. This is immaterial, as the location of the impulse is more or less arbitrary for an impulsive approximation of continuous-thrust, save for the case of the last segment in any half-phase where placing the maneuver on the right-hand boundary results in it occurring exactly at the match-point. When both half-phases are considered, this results in the burn at the match-point having a maximum *potential* size that is twice as large as the others. This is not a major concern, however, as the purpose of bounded-impulse methods is to produce an accurate estimation of the total mass requirement of a mission, and not necessarily the exact geometry of its trajectory. This problem also reduces asymptotically with the use of more control nodes.

Computation of the match-point constraint partials is carried out in a similar fashion to the original MGALT transcription, with the added complexity of the new χ_p decision variables.

APPLICATION: RENDEZVOUS WITH COMET 45P/HONDA-MRKOS-PAJDUŠÁKOVÁ

The problem selected to illustrate the benefits of time regularization is a notional rendezvous with the comet 45P/Honda-Mrkos-Pajdušáková. This is a short-period comet with a period of approximately 5.25 years. We consider a direct flight to the comet, with no intermediate flybys. This rendezvous problem was solved once using the MGALT transcription (Figure 1) and then a second time using the MGALTS transcription (Figure 2) using the exact same configuration parameters. The NLP objective function was the minimization of the propellant consumed.
Specific information about power modeling and throttle logic used is omitted here but is available, and adheres to Discovery class mission proposal requirements.[13,14]

Figures 1 and 2 show that the optimizer arrives at two answers that differ by less than one percent in terms of mass delivered to the comet. This is a testament to just how accurate the MGALT transcription is at approximating a mission's mass requirements. The major difference between the two solutions is the flight time required to make the transfer. The MGALT trajectory requires 10.10 years, whereas the MGALTS completes the rendezvous in only 7.96 years. The throttle histories depicted in Figures 3 and 4 shed light on why this is the case. The MGALTS trajectory features a much later launch date, and even arrives earlier at the target. It is able to achieve this due to greater number of control points located near periapsis for that transcription. The clustering of control nodes there allows the pump-up maneuver to happen more efficiently, meaning the spacecraft can match the energy of the comet's orbit in a much

Table 1. 45P/Honda-Mrkos-Pajdušáková rendezvous mission parameters

Parameter	Value
Maximum allowed initial mass	4000 kg
Earliest allowed launch date	August 27th, 2016
Launch window	5 years
Maximum flight time	unbounded
Latest allowed arrival date	January 1st, 2030
Launch vehicle	Atlas V (555) NLS-2
Maximum launch C3	21.7156 km^2/s^2
Launch declination bounds	$[-28.5^\circ, 28.5^\circ]$
Arrival type	rendezvous
Thruster	2 x NEXT TT11 high thrust
Throttle logic	minimum number of thrusters
Thruster duty cycle	0.95
Solar power coefficients	$\gamma_0 = 1.32077\ \gamma_1 = -0.10848$ $\gamma_2 = -0.11665\ \gamma_3 = 0.10843$ $\gamma_4 = -0.01279$
Spacecraft bus power requirement coefficients	$a_{s/c} = 1.0$ $b_{s/c} = 0.0$ $c_{s/c} = 0.0$
Solar array BOL power (launch at 1 A.U.)	40.0 kW
Power margin (δ_{power})	15%
Post-launch checkout coast	60 days
Number of segments per phase	200
Ephemeris	SPICE
SNOPT feasibility tolerance	1.0e-5
SNOPT optimality tolerance	1.0e-4
Objective function	maximize final mass

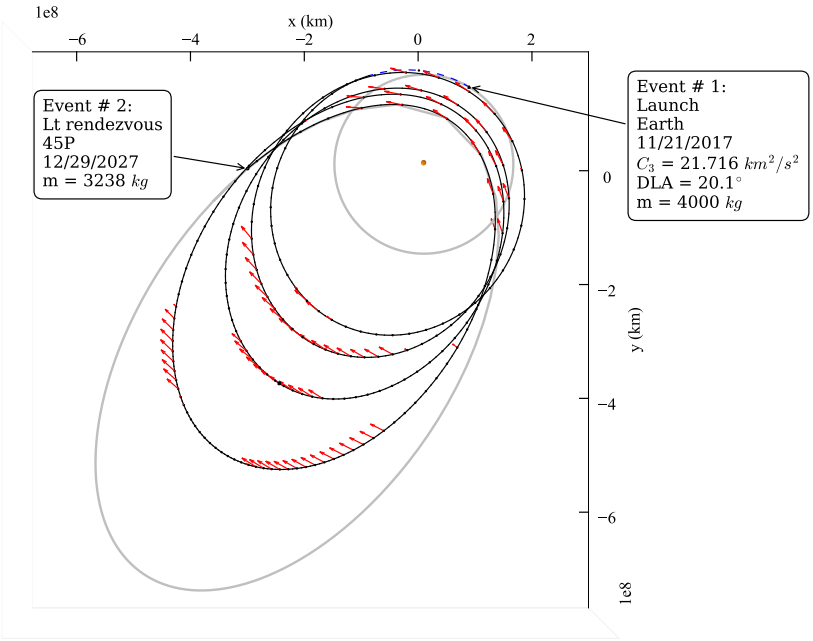

Figure 1. Rendezvous with 45P using MGALT with 200 segments, $\Delta t_{\text{mission}} = 3690$ days

shorter time. The MGALT solution on the other hand is not able to achieve the same energy change per periapsis passage. This works out in a particularly unlucky way for this mission as it results in the spacecraft having to make an entire extra revolution of the sun in order to carry out the rendezvous. Since the MGALT node placement is less optimal, the optimizer adds an additional revolution in order to place the maneuvers more effectively, which in turn requires that the spacecraft launch earlier.

By increasing the number of control nodes for the MGALT model, a solution in the same family as the MGALTS solution can be obtained due to the increased number of nodes at periapsis. Figure 5 shows the new MGALT solution,

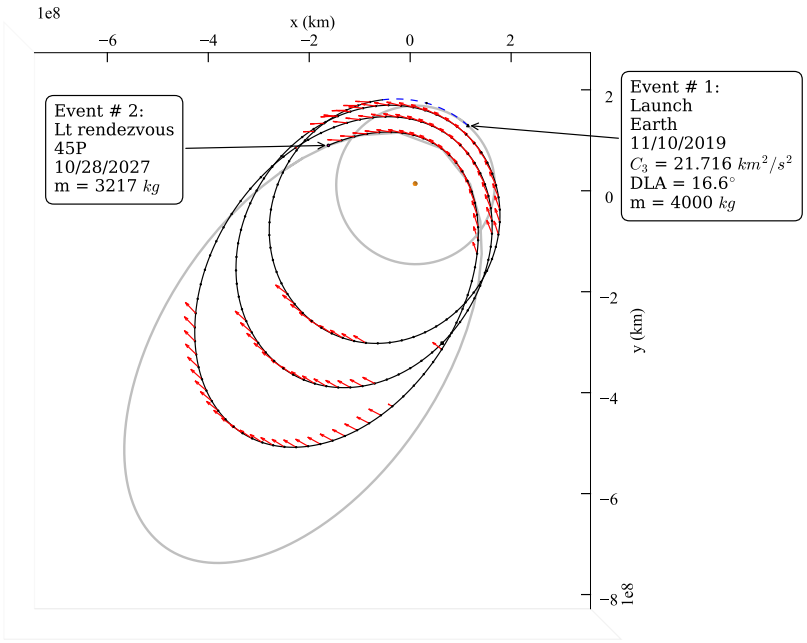

Figure 2. Rendezvous with 45P using time-regularized MGALTS with 200 segments, $\Delta t_{\text{mission}} = 2909$ days

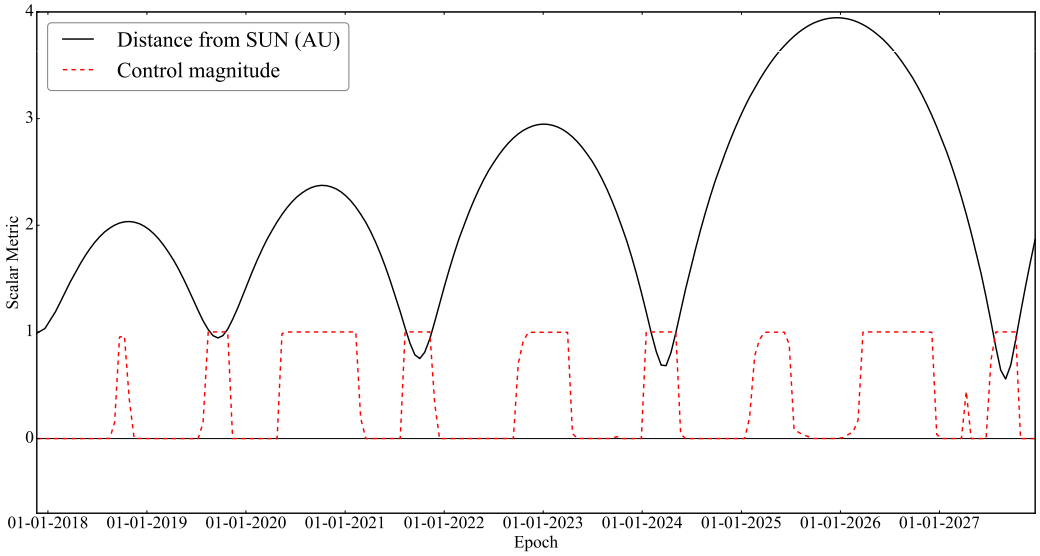

Figure 3. MGALT throttle magnitude and distance from the sun as a function of time.

this time using 400 segments instead of 200. Increasing the segment count by degrees will eventually yield a trajectory with a more comparable flight time to the MGALTS solution.

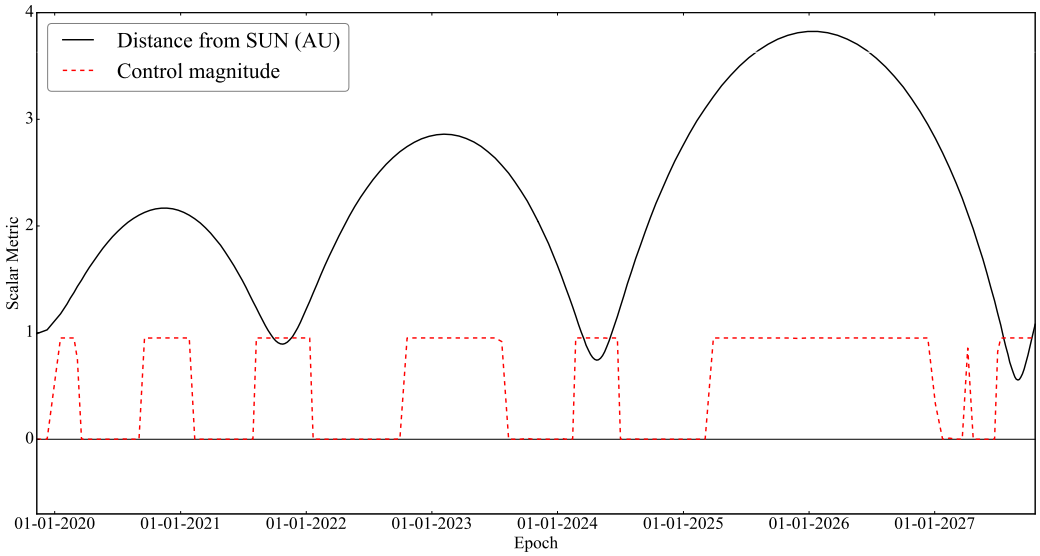

Figure 4. MGALTS throttle magnitude and distance from the sun as a function of time.

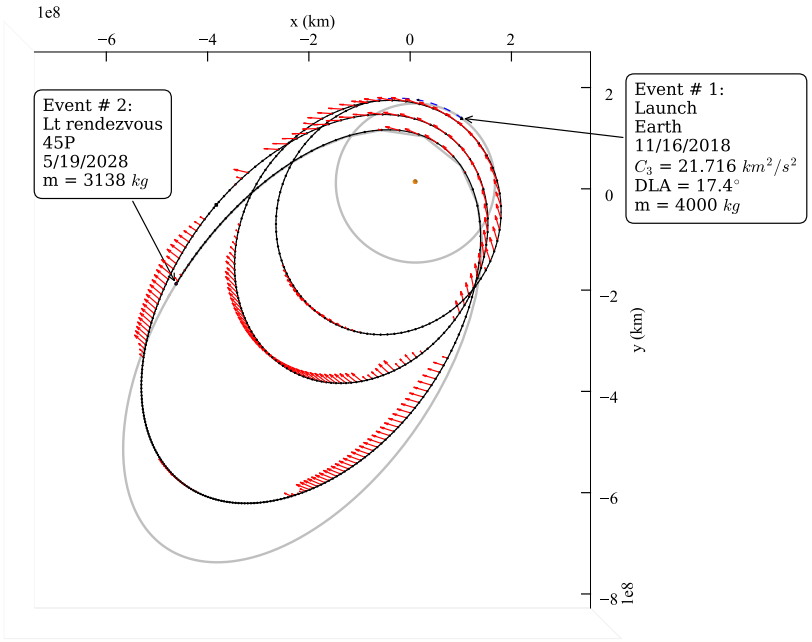

Figure 5. Rendezvous using the time-regularized MGALT transcription with 400 segments

CONCLUSION

Time-regularization of the bounded-impulse Kepler low-thrust model has been achieved using an exact, non-iterative analytic algorithm. It is also possible to obtain analytic partial derivatives for the nonlinear constraints defining this

transcription. This methodology is particularly effective at solving trajectory problems requiring large eccentricity changes, especially those requiring multiple revolutions of the central body. By replacing time with the generalized anomaly as the independent propagation variable, the control nodes of the MGALT model can be distributed in an even geometric fashion, increasing the number of nodes near periapsis. This important feature of the model allows for a discrete control history that more closely matches the optimal one that could be found using the necessary conditions of the Calculus of Variations. This difference can lead to trajectory solutions with a similar cost function value to those produced by the MGALT model, but vary significantly in topology. This is illustrated by the example comet rendezvous problem that was solved in this paper where a nearly identical cost function (within 1%) was achieved with MGALT and MGALTS, however, the flight time of the MGALTS solution was slightly over two years shorter.

APPENDIX

Kepler Propagation with Universal Functions

The transcription described in this paper utilizes Keplerian two-body propagation using the Lagrange coefficients,[12]

$$\begin{bmatrix}\mathbf{r}_k\\ \mathbf{v}_k\end{bmatrix} = \begin{bmatrix}F_k & G_k\\ \dot{F}_k & \dot{G}_k\end{bmatrix}\begin{bmatrix}\mathbf{r}_{k-1}\\ \mathbf{v}_{k-1}\end{bmatrix}. \tag{3}$$

For use with a numerical optimizer, it is generally beneficial to use a two-body propagation method capable of robustly propagating any orbit initial condition (i.e. elliptical, parabolic or hyperbolic) initialized by a search method. For this reason, a propagation method based on universal orbit variables is employed. The universal variables are defined according to the energy regime of the orbit:

$$\alpha_k > 0 \begin{cases} U_{1_k} = \chi_k(1 - y_k S_k) \\ U_{2_k} = \chi_k^2 C_k \\ U_{3_k} = \chi_k^3 S_k \\ U_{0_k} = 1 - \alpha_k U_{2_k} \end{cases} \tag{4}$$

where,

$$\alpha_k = \frac{1}{a_k} = \frac{2}{r_k} - \frac{v_k^2}{\mu} \tag{5}$$

$$y_k = \alpha_k \chi_k^2 \tag{6}$$

$$C_k = \frac{1}{y_k}\left(1 - \cos(\sqrt{y_k})\right) \tag{7}$$

$$S_k = \frac{1}{y_k^3}\left(\sqrt{y_k} - \sin(\sqrt{y_k})\right) \tag{8}$$

$$\alpha_k < 0 \begin{cases} U_{0_k} = \cosh(\sqrt{-\alpha_k}\chi_k) \\ U_{1_k} = \frac{1}{\sqrt{-\alpha\chi_k}}\sinh(\sqrt{-\alpha_k}\chi_k) \\ U_{2_k} = \frac{1}{\alpha_k}(1 - U_{0_k}) \\ U_{3_k} = \frac{1}{\alpha_k}(\chi_k - U_{1_k}) \end{cases} \tag{9}$$

$$\alpha_k = 0 \begin{cases} U_{0_k} = 1 \\ U_{1_k} = \chi_k \\ U_{2_k} = \frac{1}{2}U_{1_k}\chi_k \\ U_{3_k} = \frac{1}{3}U_{2_k}\chi_k \end{cases} \tag{10}$$

The propagation time Δt_k associated with a corresponding change in generalized anomaly χ_k is computed as follows:

$$\Delta t_k = \frac{1}{\sqrt{\mu}}\left(r_0 U_1 + \sigma_0 U_2 + U_3\right) \tag{11}$$

$$\frac{\partial \Delta t_k}{\partial \chi_k} = \frac{1}{\sqrt{\mu}}\left(r_0\frac{\partial U_1}{\partial \chi_k} + \sigma_0\frac{\partial U_2}{\partial \chi_k} + \frac{\partial U_3}{\partial \chi_k}\right) \tag{12}$$

where,

$$\sigma_k = \frac{\mathbf{r}_k \cdot \mathbf{v}_k}{\sqrt{\mu}} \tag{13}$$

The distance from the central body at the end of the propagation segment is:

$$r_{k+1} = r_k U_{0_k} + \sigma_k U_{1_k} + U_{2_k} \tag{14}$$

The Lagrange coefficients and their derivatives are given by:

$$F_k = 1 - \frac{U_{2_k}}{r_k} \tag{15}$$

$$\frac{\partial F_k}{\partial \chi_k} = -\frac{1}{r_k}\frac{\partial U_{2_k}}{\partial \chi_k} \tag{16}$$

$$\dot{F}_k = -\frac{\sqrt{\mu}}{r_{k+1} r_k} U_{1_k} \tag{17}$$

$$\frac{\partial \dot{F}_k}{\partial \chi_k} = \frac{\sqrt{\mu}}{r_k}\left(\frac{U_{1_k}}{r_{k+1}^2}\frac{\partial r_{k+1}}{\partial \chi_k} - \frac{1}{r_{k+1}}\frac{\partial U_{1_k}}{\partial \chi_k}\right) \tag{18}$$

$$G_k = \frac{1}{\sqrt{\mu}}\left(r_k U_{1_k} + \sigma_k U_{2_k}\right) \tag{19}$$

$$\frac{\partial G_k}{\partial \chi_k} = \frac{1}{\sqrt{\mu}}\left(r_k \frac{\partial U_{1_k}}{\partial \chi_k} + \sigma_k \frac{\partial U_{2_k}}{\partial \chi_k}\right) \tag{20}$$

$$\dot{G}_k = 1 - \frac{U_{2_k}}{r_{k+1}} \tag{21}$$

$$\frac{\partial \dot{G}_k}{\partial \chi_k} = \frac{U_{2_k}}{r_{k+1}^2}\frac{\partial r_{k+1}}{\partial \chi_k} - \frac{1}{r_{k+1}}\frac{\partial U_{2_k}}{\partial \chi_k} \tag{22}$$

where,

$$\frac{\partial r_{k+1}}{\partial \chi_k} = r_k \frac{\partial U_{0_k}}{\partial \chi_k} + \sigma_k \frac{\partial U_{1_k}}{\partial \chi_k} + \frac{\partial U_{2_k}}{\partial \chi_k} \tag{23}$$

$$\dot{r}_{k+1} = r_k \dot{U}_{0_k} + \sigma_k \dot{U}_{1_k} + \dot{U}_{2_k} \tag{24}$$

$$\sigma_{k+1} = \sigma_k U_{0_k} + \left(1 - \alpha_k r_k\right) U_{1_k} \tag{25}$$

$$\frac{\partial U_{0_k}}{\partial \chi_k} = -\alpha_k U_{1_k}; \quad \frac{\partial U_{n_k}}{\partial \chi_k} = U_{n-1_k} \quad n = 1, 2, ... \tag{26}$$

ACKNOWLEDGMENTS

Inspiration to develop the iteration-free Kepler propagator was in part brought on after seeing a recent AAS conference presentation by Ricardo Restrepo and Ryan Russell (AAS 16-523).

REFERENCES

[1] J. Sims, P. Finlayson, E. Rinderle, M. Vavrina, and T. Kowalkowski, "Implementation of a Low-Thrust Trajectory Optimization Algorithm for Preliminary Design," *AIAA/AAS Astrodynamics Specialist Conference, AIAA Paper 2006-6746*, August 2006.

[2] T. T. McConaghy, T. J. Debban, A. E. Petropoulos, and J. M. Longuski, "Optimization of Low-Thrust Trajectories with Gravity Assists," *Journal of Spacecraft and Rockets*, Vol. 40, No. 2, 2003, pp. 380 – 387, 10.2514/2.3973.

[3] "PaGMO (Parallel Global Multiobjective Optimizer)," March 2012. http://pagmo.sourceforge.net/pagmo/index.html.

[4] J. A. Sims and S. N. Flanagan, "Preliminary Design of Low-Thrust Interplanetary Missions," *AAS/AIAA Astrodynamics Specialist Conference, AAS Paper 99-338*, Girdwood, Alaska, August 1999.

[5] J. A. Englander, D. H. Ellison, and B. A. Conway, "Global Optimization of Low-Thrust, Multiple-Flyby Trajectories at Medium and Medium-High Fidelity," *AAS/AIAA Space Flight Mechanics Meeting, AAS Paper 14-309, Santa Fe, NM*, January 26 - 30 2014.

[6] D. H. Ellison, B. A. Conway, and J. A. Englander, "Numerical Computation of a Continuous-Thrust State Transition Matrix Incorporating Accurate Hardware and Ephemeris Models," *AAS/AIAA Space-Flight Mechanics Meeting, Williamsburg, VA*, January 11 - 15 2015.

[7] "General Mission Analysis Tool," September 2014. http://gmatcentral.org/display/GW/GMAT+Wiki+Home.

[8] G. J. Whiffen, "Static/Dynamic Control for Optimizing a Useful Objective," United States Patent No. 6 496 741, December, 22 2002. Filed March 25, 1999.

[9] G. J. Whiffen, "Mystic: Implementation of the Static Dynamic Optimal Control Algorithm for High-Fidelity, Low-Thrust Trajectory Design," *AIAA/AAS Astrodynamics Specialist Conference and Exhibit, AIAA Paper 2006-6741*, Keystone, Colorado, August 21-24 2006, 10.2514/6.2006-6741.

[10] E. Pellegrini, R. P. Russell, and V. Vittaldev, "F and G Taylor Series Solutions to the Stark and Kepler Problems with Sundman Transformations," *Celestial Mechanics and Dynamical Astronomy*, Vol. 118, No. 4, 2014, pp. 355–378, 10.1007/s10569-014-9538-7.

[11] C. H. Yam, D. Izzo, and F. Biscani, "Towards a high fidelity direct transcription method for optimisation of low-thrust trajectories," 4^{th} *International Conference on Astrodynamics Tools and Techniques*, 2010, pp. 1–7.

[12] R. H. Battin, *An Introduction to the Mathematics and Methods of Astrodynamics, Revised Edition*. Reston, Virginia: American Institute of Aeronautics and Astronautics Inc., 1999.

[13] "NASAs Evolutionary Xenon Thruster (NEXT) Ion Propulsion GFE Component Information Summary for Discovery Missions July 2014," July 2014. http://discovery.larc.nasa.gov/discovery/pdf_files/20-NEXT-C_AO_Guidebook_11July14.pdf.

[14] D. H. Ellison, B. A. Conway, J. A. Englander, and M. T. Ozimek, "Partial Derivative Computation for Bounded-Impulse Trajectory Models Using Two-Sided Direct Shooting. Part 2: Application," *To appear in the Journal of Guidance, Control, and Dynamics*, Vol. XXX, No. X, XXXX, pp. XXX–XXX, X.